DOI 10.1007/s11182-017-1116-5

Russian Physics Journal, Vol. 60, No. 4, August, 2017 (Russian Original No. 4, April, 2017)

THE EFFECT OF HIGH-TEMPERATURE ANNEALING ON THE STRUCTURAL-PHASE STATE OF ULTRAFINE GRAIN STEEL 0.1C–2V–1Ti–Fe

N. A. Popova,[1,2] E. L. Nikonenko,[1,3] N. R. Sizorenko,[1] and N. A. Koneva[1] UDC 669.24: 539.25

Using transmission electron microscopy and X-ray diffraction analysis, the structural-phase state of steel 0.1C–2V–1Ti–Fe, deformed by the SPD methods and subjected to high-temperature annealing at the temperatures 600 and 700°C, is investigated. The influence of the steady temperature on the grain size, steel phase composition, carbide transformations, carbide particle size and distribution density, carbon distribution, and fine-structure parameters are determined. A special focus is made on the sources of internal stress.

Keywords: steel, grain, carbides, dislocations, scalar dislocation density, geometrically necessary and statistically stored dislocations, crystal lattice curvature-torsion, long-range stresses.

INTRODUCTION

At present it is well known that application of ultrafine-grained (UFG) materials produced by the methods of severe plastic deformation (SPD) allows considerably improving their strength characteristics [1–16]. During grain refinement changes occur in dislocation density, crystal lattice curvature-torsion, and other structural characteristics of metallic materials [17–21]. During annealing such processes are observed in UFG-steels as grain-size increase [10, 11, 16], phase transformations followed by redistribution of the elements in the steel matrix [15, 16], precipitation of carbide particles [10, 11, 16], their phase transformations, and changes in their size and distribution density [16]. The annealing temperature also affects the fine-structure parameters of UFG-steel – scalar dislocation density and internal stresses [16]. The changes in structural-phase states of UFG-steels can significantly influence their hardening. The purpose of this work is therefore to investigate the effects of high-temperature annealing on the structural-phase state of 0.1C–2V–1Ti–Fe steel manufactured by the process of equal-channel angular pressing (ECAP).

1. MATERIAL AND EXPERIMENTAL PROCEDURE

The experimental material was structural steel of the 0.1C–2V–1Ti–Fe grade (0.10% C; 0.07% Cr; 1.12% Mn; 0.20% Si; 0.10% P; 0.07% Ni; 0.06% Al; 0.07% Ti; 0.08% V). The steel specimens were subjected to deformation using the ECAP process in the B_C mode [2]. In this process they underwent shear deformation by compression in two channels of equal diameters crossing at the angle $\Phi = 120°$ at the temperature $T = 400$°C without any intermediate anneals. The number of passes was $N = 4$. As a result of ECAP, the specimens were shaped as rods 60 mm in length and 10 mm in diameter. The equivalent strain achieved by ECAP was $\varepsilon = 2.7$. After that the specimens were annealed at two

[1]Tomsk State University of Architecture and Building, Tomsk, Russia, e-mail: natalya-popova-44@mail.ru; snr1952@mail.ru; koneva@tsuab.ru; [2]Institute of Strength Physics and Materials Science of the Siberian Branch of the Russian Academy of Sciences, Tomsk Russia; [3]National Research Tomsk Polytechnic University, Tomsk, Russia, e-mail: vilatomsk@mail.ru. Translated from Izvestiya Vysshikh Uchebnykh Zavedenii, Fizika, No. 4, pp. 53–60, April, 2017. Original article submitted January 27, 2017.

TABLE 1

Phase	Crystal lattice types	Space group	Crystal lattice parameters, nm
α-phase	BCC	*Im*3*m*	a = 0.2867–0.2868
α′-phase	BCC	*Im*3*m*	a = 0.2867
γ-phase	FCC	*Fm*3*m*	a = 0.3586
Fe_3C	Orthorhombic	*Pnma*	a = 0.5080, b = 0.6774, c = 0.4520
V_2C	Orthorhombic	*Pbcn*	a = 0.4577, b = 0.5742, c = 0.5037
$M_{23}C_6$	FCC	*Fd*3*m*	a = 1.0585
TiC	FCC	*Fm*3*m*	a = 0.4330

temperatures: 600°C (1 h) and 700°C (1 h). Their structure and phase states were examined both in the initial state (after ECAP) and after annealing.

The morphology and structural-phase state of the steel were investigated by the methods of transmission electron diffraction microscopy (TEM) and X-ray diffraction analysis (XRD). TEM studies were performed in an EM-125 electron microscope at the accelerating voltage 125 kV. The standard magnification in the electron microscope column was a multiple of 25000. The X-ray diffraction studies were carried out in a DRON-3 X-ray diffractometer using K_β high-intensity X-ray radiation. The reflections were registered onto the diagram tape using a proportional counter.

The phase analysis was carried out using the images validated by the microdiffraction patterns and dark-field images obtained in the respective reflections. We measured the grain size, the volume fractions (P_V) of the morphological components of steel, the carbide particle size (d), their distribution density ($1/r$) and volume fractions (δ), the scalar density of dislocations (ρ), the density of geometrically necessary (ρ_G) and statistically stored (ρ_S) dislocations, the crystal lattice curvature-torsion amplitude (χ), and the amplitude of long-range internal stress fields σ_{lr}. The linear dimensions and scalar dislocation density were determined by the secant method via standard techniques. The density of geometrically necessary dislocations ρ_G was calculated from the amplitude of the crystal lattice curvature-torsion χ [20]. The density of statistically stored dislocations was calculated as $\rho_S = \rho - \rho_G$ [20]. The amplitude of the crystal lattice curvature-torsion (χ) was measured from the local misorientation gradient [22].

The XRD data were used to determine the content of carbon and doping elements in the solid solution, the crystal lattice parameter of steel, and the sizes of blocks of coherently diffracting domains and Type II microstresses (compression-torsion microstresses). All the data obtained were subjected to a statistical analysis.

2. RESULTS AND DISCUSSION

2.1. Phase composition

The investigations performed in this work demonstrated that there are three types of solid solutions in the steel in different states (initial, after ECAP, and after high-temperature annealing): α-phase – ferrite, α′-phase – martensite, and γ-phase – retained austenite. The crystal structure of α- and α′-phases is cubic. The crystal lattice parameters, determined by XRD, the space groups, and the crystal lattice types are listed in Table 1. The α- and α′-phases differ in their morphology (in what follows they will be described in more detail), and the γ-phase has an FCC-crystal lattice. The crystal lattice parameter of this phase is also presented in Table 1. The content of γ-phase is small; it is present in one state only – after tempering at 700°C.

There are four types of carbides in the steel: Fe_3C (cementite), V_2C, $M_{23}C_6$ and TiC. The cementite Fe_3C has an orthorhombic crystal lattice. The space group of Fe_3C and the parameters of its crystal lattice are also presented in Table 1: Fe_3C is present in the initial state of the steel only. The carbide V_2C has an orthorhombic lattice, its space group and the crystal lattice parameters are also listed in Table 1. This carbide is present in the annealed steel only, its volume fraction being independent of the annealing temperature. The carbide $M_{23}C_6$ represents a complex cubic carbide composition $(Fe, Mn)_{23}C_6$, having an FCC-based cubic lattice. Its space group and the crystal lattice parameters are also

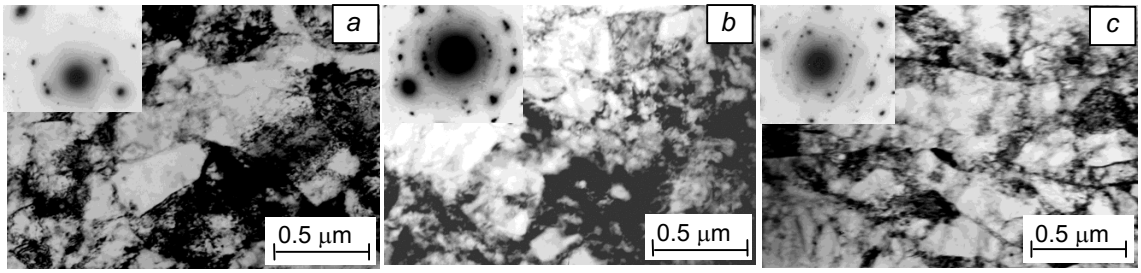

Fig. 1. TEM images of three types of micrograins and their diffraction patterns in 0.1C–2V–1Ti–F steel in the initial state: fine isotropic grains (*a),* ultrafine isotropic grains *(b),* and a mixture of ultrafine isotropic and anisotropic grains (*c*).

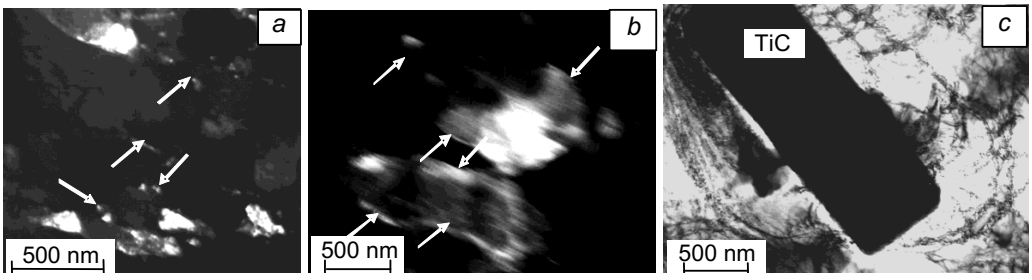

Fig. 2. TEM images of carbide particles: Fe_3C particles located along the boundaries (indicated by white arrows) of isotropic (*a*) and anisotropic (*b*) grains of α- and TiC (*c*): dark- (*a, b)* and bright-field *(c*) images.

given in Table 1. Similarly to V_2C, it is found in the annealed steel only, but due to a considerable content of Mn it partially loses its stability after high-temperature annealing at 700°C. This is validated by the γ-phase formation during annealing at 700°C, which consumes part of Mn. The carbide TiC has an FCC crystal structure (see Table 1 for its crystal lattice and space group data). This carbide is found in all steel states. There is sufficient ground to believe that during ECAP it destroys only partially or does not decompose at all. This is an unexpected outcome, for during ECAP precipitates of all phases generally decompose [2, 15, 16].

2.2. Structure and phase composition of the initial steel

In the initial state the main volume of the steel is represented by α-phase – a solid solution based on FCC-Fe. The relative volume of α-phase is close to 0.99. From the morphological perspective it is fine crystalline grain structure that can be classified into three types. The first type – dislocation-free fine isotropic grains (Fig. 1*a*), the second type is presented by ultrafine isotropic grains (Fig. 1*b*), and the third type contains anisotropic grains in addition to ultrafine isotropic microparticles (Fig. 1*c*).

The average size of isotropic grains of the first type is found to be (334 ± 101) nm. The diffraction patterns obtained from such regions of the material reveal the presence of fine-grained polycrystalline structure. This is indicated by a characteristic arrangement of reflections across the ring. The average grain size of the second type (Fig. 1*b*) is found to be (110 ± 40) nm. Due to grain structure refinement, compared to that presented in Fig. 1*a*, the diffraction fringes are sharper (Fig. 1*b*). Anisotropic grains of the third type are presented in Fig. 1*c*. It is evident that the grains are elongated. Their transverse size is (316 ± 148) nm. Notice the sharp contrast from the axial boundaries of the grains, implying their relatively defect-free structure. In the axial direction the grains are several-fold longer than in the transverse one.

TABLE 2. Dimensions of Grains and Carbide Particles of Steel 0.1C–2V–1Ti–F in the Initial and Tempered States

Specimen state	Grain size, nm		Thickness of γ-phase interlayer, nm	Carbide particle dimensions, nm/Interparticle spacing, nm			
	α-phase	α′-phase		Fe_3C	V_2C	$M_{23}C_6$	TiC
Initial	330	–	–	20 / 120	–	–	1700 / 800
Tempering at 600°C, 1 h	2580	–	–	–	20 / 120	120 / 500	
Tempering at 700°C, 1 h	3280	610	12	–	12 / 70	40 / 200	

TABLE 3. Quantitative Characteristics of Fine Structure

Specimen state	Dislocation density	Amplitude of internal stresses $\sigma_{l\text{-}r}$, MPa		Amplitude of crystal lattice curvature-torsion χ, m^{-1}
		geometrically necessary ρ_G, m^{-2}	statistically stored ρ_S, m^{-2}	
Initial	$3.5\cdot10^5$	$1.40\cdot10^{14}$	$2.1\cdot10^{15}$	750
Tempering at 600°C, 1 h	$0.4\cdot10^5$	$0.18\cdot10^{15}$	$0.06\cdot10^{15}$	270
Tempering at 700°C, 1 h	$0.5\cdot10^5$	$0.19\cdot10^{15}$	$0.03\cdot10^{14}$	280

The carbide particles observed in the initial steel are represented by cementite Fe_3C (Fig. 2*a*, *b*) and titanium carbide TiC (Fig. 2*c*). The particles of Fe_3C are shaped as thin interlayers located along the boundaries of micrograins. The average particle size is found to be 20×120 nm and their volume fraction in the initial steel − 0.6%. The carbide particles TiC represent separate plate-like formations. They are not associated with the grain boundaries or the dislocation structure of the matrix. The average particle size is 0.8×1.7 μm and the volume fraction is ~1%.

Thus the quantitative estimation performed (Table 2) validate that the initial SPD steel used in this work has ultrafine-grained structure containing nanosized carbides.

The investigations have demonstrated that the initial steel possesses a comparatively high scalar dislocation density ρ. The average scalar dislocation density in the material is found to be $3.5\cdot10^{15}$ m^{-2}. It should be noted that the value of ρ is independent of either type or size of micrograins. The dislocation structure represents dense dislocation networks.

The initial steel in α-phase is characterized by considerably large curvature-torsion of the crystal lattice χ. The measurements have demonstrated that on average it is $\chi = 3.5\cdot10^5$ m^{-1}. This suggests that the density of geometrically necessary dislocations [19] would be $\rho_G = 1.4\cdot10^{15}$ m^{-2}. The density of the statistically stored dislocations $\rho_S = \rho - \rho_G$ would then be equal to $2.1\cdot10^{15}$ m^{-2}. The presence of this number of ρ_G suggests that the dislocation structure is polarized. Polarization of the dislocation structure gave rise to the formation of internal (long-range) stresses whose amplitude was found to be equal to 750 MPa (Table 3). It has to be underlined that such stresses persist in the vicinity of the internal stress sources only (micrograin boundaries, carbide particles) and do not engage the entire material.

2.3. Steel structure and phase composition after its 1-hour annealing at 600°C

Steel annealing at the temperature 600°C gave rise to several processes. The first is recovery (or recrystallization) of the grain structure. The grains have considerably (by nearly an order of magnitude) increased in their dimensions (Table 2) and their values became as large as (2.6 ± 1.5) μm. It is evident in Fig. 3, presenting typical grain structure, that in addition to large grains there are fine grains near their junctions. The diffraction pattern has also changed due to the grain growth. It now has an appearance characteristic of single crystals. Note that it contains grains of anisotropic shapes. These grains were inherited from the anisotropic grains observed in Fig. 1*c*.

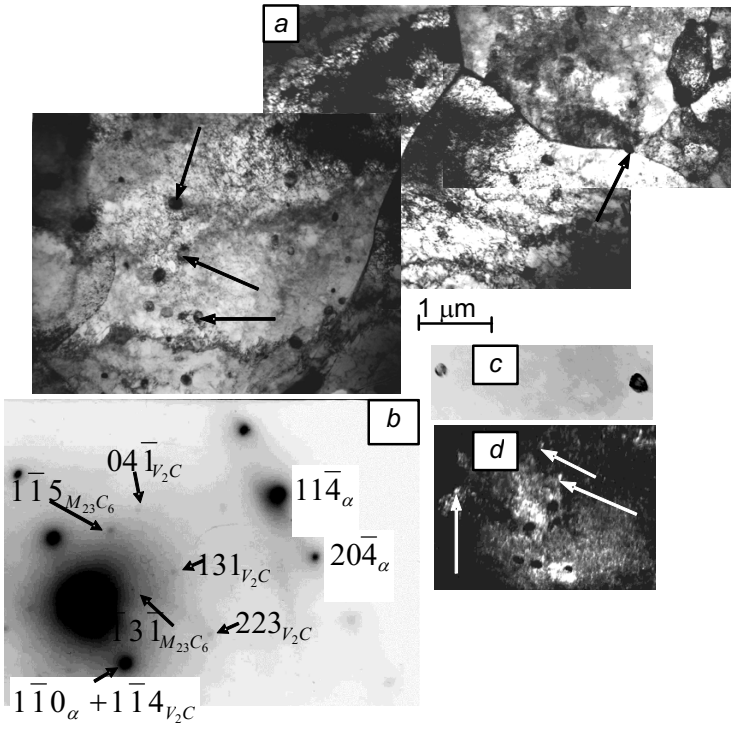

Fig. 3. Typical grain structure of 0.1C–2V–1Ti–F steel after annealing at 600°C, 1 h. Precipitation of carbide particles $M_{23}C_6$ inside the grains and at their boundaries (black arrows in (*a*)) and particles of V_2C on dislocations (white arrows in (*d*)): bright-field image (*a*), microdiffraction pattern (*b*), and dark-field images obtained in the reflections of $[1\,\bar{1}5]$ $M_{23}C_6$ and $[1\,\bar{1}0]\alpha + [1\,\bar{1}4]$ V_2C carbides, respectively (*c*, *d*).

The second process is precipitation of carbides and carbide transformations. After annealing there is no cementite in the steel. The main carbide is cubic $M_{23}C_6$, specifically $(Mn, Fe)_{23}C_6$ (Fig. 3). Its particles are found both inside the grains of α-phase and along their boundaries. The volume fraction of this carbide is about 3% and the average particle size is 120 nm (Table 2). Nearly 2/3 of its particles are concentrated in the bulk of the grains and 1/3 – along the grain boundaries. Along with $M_{23}C_6$, there is a small content (0.2%) of the V_2C carbide (Fig. 3). Its particles measure 20 nm (Table 2). They precipitate on dislocations. Both in the initial and tempered steels there are particles of TiC; note that their shapes, dimensions, location, and volume fraction are the same as those in the initial steel.

The third process taking place during tempering is the dislocation structure recovery. It has remained to be cellular, but the dislocation density has considerably decreased ($<\rho> = 0.24 \cdot 10^{15}$ m^{-2}).

The fourth process is a decrease in the amplitude of crystal lattice curvature-torsion. After annealing at 600°C, the average value of the crystal lattice curvature-torsion is found to be $\chi = 0.4 \cdot 10^5$ m^{-1}, which is approximately an order lower than that in the initial state (Table 3). The value of χ is higher near the grain boundaries and lower inside them. The density of geometrically necessary dislocations is $\rho_G = 0.18 \cdot 10^{15}$ m^{-2}, which is also about an order lower than that in the initial steel (Table 3). The density of the statistically stored dislocations is $\rho_S = 0.06 \cdot 10^{15}$ m^{-2}. A comparison of ρ_G and ρ_S (Table 3) indicates that the dislocation structure is polarized.

The investigations performed in this study have demonstrated that after annealing at 600°C, 1 h the sources of internal stresses are primarily grain junctions. It has been established that nearly 1/4 of these junctions contain junction disclinations. Secondly, their sources are grain boundaries. These boundaries account for about 50% of all boundaries present in the annealed steel. Thus, relying on the measurements performed, we have found that the amplitude of long-range internal stresses is 270 MPa, which is considerably (about a factor of 3) lower than that in the initial state of the steel (Table 3).

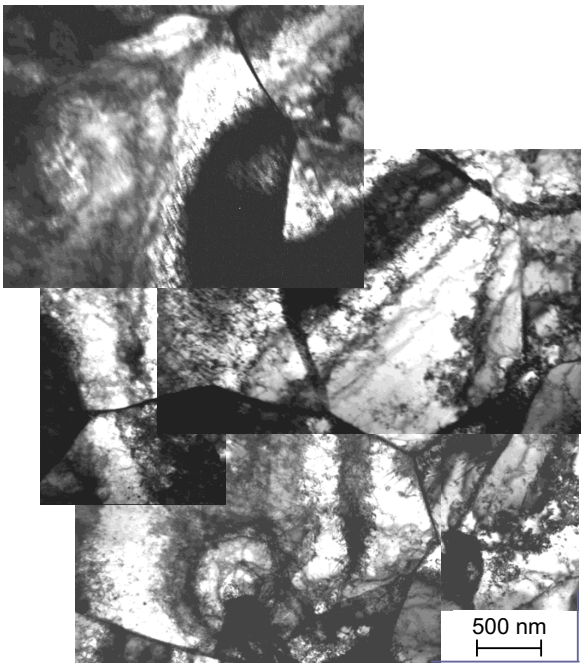

Fig. 4. Typical grain structure in 0.1C–2V–1Ti–F steel after annealing at 700°C, 1 h.

2.4. Steel structure and phase composition after its 1-hour annealing at 700°C

This thermal treatment resulted in more complex changes of the steel structure. Firstly, heating to 700°C resulted in the recovery of the grain and dislocation structure of α-phase (Fig. 4). The average grain size increased to (3.3 ± 1.5) μ (see Table 2). The dislocation density decreased to the value $<\rho> = 0.2 \cdot 10^{15}$ m^{-1}. The grain boundaries are predominantly clear; they do not contain any carbide particles. The density of the bending extinction contours increased compared to the annealing treatment at 600°C and so did the crystal lattice curvature-torsion χ. It was found to be equal to $0.5 \cdot 10^5$ m^{-1}. The density of geometrically necessary dislocations ρ_G (Table 3) slightly increased. Thus the density of statistically stored dislocations ρ_S became still lower (Table 3).

Another difference compared to the steel annealed at 600°C consists in the carbide-phase structure. Both the size and number of carbide particles $(Mn, Fe)_{23}C_6$ at the annealing temperature 700°C decreased. The average size of the carbide particles was found to be 40 nm and the volume fraction – 0.5%. As mentioned above, this implies that this carbide partially loses its stability after the high-temperature annealing at 700°C due to a considerable content of Mn. This is validated by the formation of γ-phase at 700°C (see below), whose formation consumes part of Mn. The content of V_2C did not change, while the size of its precipitates somewhat decreased to 10–15 nm. The particles of this carbide are still located on dislocations. As before, there are TiC precipitates, whose shape, size, location, and volume fraction are the same as those in the initial state.

The third (and principal) difference of the steel structure after its annealing at 700°C compared to 600°C is the presence of the grains of the martensitic α′-phase. The grain size of α′-phase is about 600 nm, its volume fraction in the material is 3%. The grains of α′-phase are located at the junctions of α-phase and represent packed lathe martensite (Fig. 5) with a high dislocation density, $<\rho> = 30 \cdot 10^{14}$ m^{-2}. Along the lath boundaries there are interlayers of residual austenite (~0.1%) – γ-phase (Fig. 5). The grains of α′-phase appear due to two reasons: first, heating of the specimen to 700°C and, second, a local increase in the concentration of carbon near the joints of large grains of α-phase.

Annealing at 700°C for 1 hour increased the local stresses due to a partial martensitic transformation and solution of carbides. Now there are several sources of internal stress: these are primarily, the grains of α′-phase. This

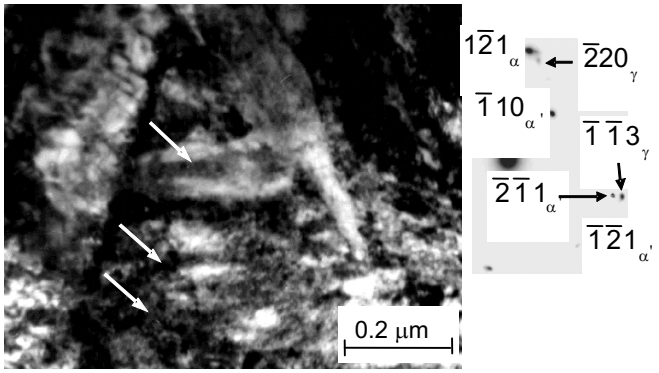

Fig. 5. Steel 0.1C–2V–1Ti–F after annealing at 700°C, 1 h. A grain of α′-phase. A packet of lath martensite (α′-phase) and its microdiffraction pattern. Interlayers of residual austenite (white arrows) – along the lathe boundaries.

concerns all grains of α′-phase. The second source is the grain joints in α-phase. At this point as many as 1/3 part of all joints present in the material are characterized by the presence of joint disclinations. The third source is formed by non-equilibrium grain boundaries in α-phase. After one-hour annealing at 700°C, 2/3 of the grain boundaries become non-equilibrium. On the other hand, the value of long-range internal stresses compared to annealing at 600°C increases insignificantly (see Table. 3).

2.5. Redistribution of carbon during steel tempering

The distribution of carbon in α-phase is a special and very important issue. It was mentioned above that the carbide phases present in the initial steel are cementite Fe_3C (0.6%) and titanium carbide TiC (1%). The calculations performed demonstrated that the content of carbon in these carbon phases (Fe_3C and TiC) is 0.45 at.%. The steel grade under study, according to its chemical composition, contains 0.10 wt.% C (0.45 at.% C). Thus, all of the initial carbon is present in the carbide phases. This is also supported by the XRD data: the crystal lattice parameter value in α-phase is found to be a = (0.28678 ± 0.00005) nm, which corresponds to $a_{\alpha\text{-Fe}}$. This suggests that there is no carbon in the solid solution.

Tempering of the steel at 600°C for 1 hour resulted in redistribution of the carbon phases. Now the carbide phases are as follows: vanadium carbide, V_2C (0.2%), complex cubic carbide, $M_{23}C_6$ (2.5%) and, as in the initial state, titanium carbide, TiC (1%). The calculation performed in this work demonstrated the carbon content in these carbide phase to be the same as in the initial state, 0.45 at.%. The value of the crystal lattice parameter also corresponds to $a_{\alpha\text{-Fe}}$ (a = (0.28678 ± 0.00005) nm). All this implies that the entire content of carbon is also in the carbon phase.

The calculation of the carbon balance in the experimental steel after its one-hour annealing at 700°C demonstrates that up to 0.25 at.% of carbon is found in the carbides. The rest (~0.2 at.%) is found on the crystal-lattice defects. It should be noted that the value of the crystal lattice parameter in steel tempered at 700°C is a = (0.28672 ± 000005) nm, which is also close to the lattice parameter of pure α-Fe, implying the absence of carbon in the solid solution.

2.6. Effect of high-temperature tempering on the structural-phase state of steel

The numerical data presented above (see Table 2) suggest that the grain structure of 0.1C–2V–1Ti–F steel in the initial state (following ECAP) and subsequent one-hour high-temperature anneals at 600 and 700°C represents a relatively fine-grained material. The size of the grains in α-phase in the initial state (after ECAP) is ~0.3 μm and that after subsequent anneals – 2–3 μm. The coherently diffracting domains measured in the steel in its different states using

the EXD method were found to be equal to 30–50 nm and the distance between the dislocations – 20–70 nm. The X-ray data clearly indicate the block structure actually confined between dislocations. The carbides are also fine grained. Their sizes lie within the range 12–120 nm and mainly localize in the interval 20–40 nm. This suggests nanometric dimensions of the fine structure and carbide phases. All these data indicate that despite the high-temperature tempering giving rise to recovery (recrystallization), the structure remains to be fine grained.

Thus, an analysis of these findings demonstrates that an increased annealing temperature cannot always give rise to recovery. On the contrary, tempering at the temperature close to that of a martensitic transformation can give rise to a few hardening processes. Firstly, it is the martensitic transformation and the precipitation of α′-phase. Secondly, it is the accelerated solution of carbides followed by the redistribution of carbon atoms and the increase in internal stresses. Thirdly, it is the transfer of certain carbon atoms onto defects. This process pins the dislocations and can increase the number of defects at the grain boundaries. Fourthly, it is the restructuring of grain boundaries followed by their migration. A consequence of this process is an increase in the energy of grain-boundaries and internal stresses from them. These processes have been enumerated here in order to clarify the differences between the initial state of the experimental steel and that after its annealing at the temperatures 600 and 700°C.

SUMMARY

Using the methods of transmission electron diffraction microscopy and X-ray diffraction analysis, an investigation of the effect of high-temperature annealing on the structural-phase of 0.1C–2V–1Ti–F steel, manufactured by the ECAP method, has been performed. It has been shown that high-temperature annealing results in the following: 1) grain-structure recovery (recrystallization); 2) precipitation of V_2C and $M_{23}C_6$ carbides and their transformations; 3) redistribution of carbon; 4) dislocation-structure recovery; 5) decrease in the amplitude of the crystal-lattice curvature-torsion and hence internal long-range stresses. An increase in the temperature has been observed to give rise to the precipitation of the (martensitic) α′-phase, whose grains are located in the joints of the α-grains and represent packed lath martensite with high dislocation density. Along the martensitic laths there are interlayers of the residual austenite.

The concept of this work was prompted by Professor Eduard V. Kozlov.

This work has been performed within the framework of the terms of reference of the RF ministry of education and science No. 3.8320.2017/BC.

REFERENCES

1. N. I. Noskova and R. R. Mulyukov, Submicrocrystalline and Nanocrystalline Metals and Alloys [in Russian], UrB RAS, Ekaterinburg (2003).
2. R. Z. Valiev and I. V. Aleksandrov, Bulk Nanostructured Metallic Materials [in Russian], IKC Akademkniga, Moscow (2007).
3. G. A. Malygin, Phys. Solid State, **49**, No. 6, 961–982 (2007).
4. A. A. Mazilkin, V. V. Straumal, S. G. Protasova, *et al*., J. Mater. Sci., 43, No. 11, 3800–3805 (2008).
5. V. F. Terentiev, S. V. Dobatkin, D. V. Prosvirnin, *et al*., Deform. Razrush. Mater., No. 10, 30–38 (2008).
6. A. A. Zakirova, R. G. Zaripova, and V. I. Semenov, Bulletin of USATU, 11, No. 2, 123–130 (2008).
7. R. A. Andrievskii and A. M. Glaezer, Usp. Fiz. Nauk, **179**,No.4, 337–358 (2009).
8. A. A. Zakirova and R. G. Zaripova, Deform. Razrush. Mater., No. 7, 10–15 (2010).
9. E. G. Astafurova, G. G. Zakharova, E. V. Naidenkin, *et al*., J. Metals and Metallogr., **110**, No. 3, 260–268 (2010).
10. E. G. Astafurova, G. G. Zakharova, E. V. Naidenkin, *et al*., Zh. Fizich. Mezomekh., **13**, No. 4, 91–101 (2010).
11. G. G. Zakharova, E. G. Astafurova, M. S. Tukeeva, *et al*., Russ. Phys. J., **54**, No. 4, 423–429 (2011).
12. A. M. Glaezer and N. A. Shurygina, Amorphous-Nanocrystalline Alloys [in Russian], Fizmatizdat, Moscow (2013).

13. E. G. Astafurova, G. G. Mayer, M. S. Tukeeva, *et al*., Izv. Vyssh. Uchebn. Zaved. Fiz., **56**, No. 12/2, 76–81 (2013).
14. É. V. Kozlov, N. A. Popova, E. L. Nikonenko, *et. al*., Deform. Razrush. Mater., No. 3, 10–14 (2016).
15. É. V. Kozlov, A. M. Glaezer, N. A. Koneva, *et al*., Fundamental Principles of Deformation of Nanostructured Materials (Ed. A. M. Glaezer) [in Russian], Fizmatlit, Moscow (2016).
16. É. V. Kozlov, N. A. Koneva, N. A. Popova, *et al*., New-Generation Multifunctional Structural Materials (Ed. V. E. Gromov)[in Russian], Centr. SibSU Publ., Novokuznetsk (2015).
17. É. V. Kozlov, N. A. Koneva, and N. A. Popova, Russian Metallurgy (Metally), No. 10, 867–873 (2010).
18. É. V. Kozlov, N. A. Koneva, and N. A. Popova, Zh. Fizich. Mezomekh., **12**, No. 4, 93–103 (2009).
19. É. V. Kozlov, L. I. Trishkina, N. A. Popova, and N. A. Koneva, Zh. Fizich. Mezomekh., **14**, No. 3, 95–110 (2011).
20. N. A. Koneva, N. A. Popova, and É. V. Kozlov, Perspekt. Mater., No. 12, 238–243 (2011). (Inorganic Materials).
21. É. V. Kozlov, N. A. Koneva, and N. A. Popova, Lettr. Mater., No. 3, 113–117 (2013).
22. É. V. Kozlov, D. V. Lychagin, N. A. Popova, *et al*., The Physics of Strength of Heterogeneous Materials; Coll. scientific works [in Russian], Ioffe PTI, Leningrad (1988).